Genetically-encoded BRET probes shed light on ligand bias–induced variable ion selectivity in TRPV1 and P2X5/7

Yann Loïck Chappe, Sandra Pierredon, Alexandre Joushomme, Pablo Molle, André Garenne, Anne Canovi, Solène Barbeau, Florence Poulletier de Gannes, Annabelle Hurtier, Isabelle Lagroye, et al.

PNAS RESEARCH ARTICLE | PHARMACOLOGY

Genetically-encoded BRET probes shed light on ligand bias–induced variable ion selectivity in TRPV1 and P2X5/7

Yann Loïck Chappe[a], Sandra Pierredon[b], Alexandre Joushomme[a], Pablo Molle[a], André Garenne[a], Anne Canovi[a], Solène Barbeau[c], Florence Poulletier De Gannes[a], Annabelle Hurtier[a], Isabelle Lagroye[a], Thomas Ducret[c], Jean-François Quignard[c], Vincent Compan[b], and Yann Percherancier[a,1]

Edited by David Julius, University of California, San Francisco, CA; received March 25, 2022; accepted September 19, 2022

Whether ion channels experience ligand-dependent dynamic ion selectivity remains of critical importance since this could support ion channel functional bias. Tracking selective ion permeability through ion channels, however, remains challenging even with patch-clamp electrophysiology. In this study, we have developed highly sensitive bioluminescence resonance energy transfer (BRET) probes providing dynamic measurements of Ca^{2+} and K^+ concentrations and ionic strength in the nanoenvironment of Transient Receptor Potential Vanilloid-1 Channel (TRPV1) and P2X channel pores in real time and in live cells during drug challenges. Our results indicate that AMG517, BCTC, and AMG21629, three well-known TRPV1 inhibitors, more potently inhibit the capsaicin (CAPS)-induced Ca^{2+} influx than the CAPS-induced K^+ efflux through TRPV1. Even more strikingly, we found that AMG517, when injected alone, is a partial agonist of the K^+ efflux through TRPV1 and triggers TRPV1-dependent cell membrane hyperpolarization. In a further effort to exemplify ligand bias in other families of cationic channels, using the same BRET-based strategy, we also detected concentration- and time-dependent ligand biases in P2X7 and P2X5 cationic selectivity when activated by benzoyl-adenosine triphosphate (Bz-ATP). These custom-engineered BRET-based probes now open up avenues for adding value to ion-channel drug discovery platforms by taking ligand bias into account.

ion channels | molecular pharmacology | BRET | ion selectivity | ligand bias

Significance

Thanks to innovative BRET-based probes, we shed light on ligand-biased ion selectivity, a difficult-to-study ion channel–related pharmacological concept, by performing the dynamic measurements of Ca^{2+} and K^+ concentrations and ionic strength in the nanoenvironment of the TRPV1 channel during drug challenge in real-time live-cell experiments. Our results indicate that some TRPV1 antagonists display differential potencies in inhibiting CAPS-induced Ca^{2+} and K^+ fluxes. We also detect concentration- and time-dependent ligand biases in P2X7 and P2X5 cationic selectivity. These new BRET-based probes now open up avenues for adding value to ion-channel drug discovery platforms by taking ligand bias into account, thus addressing molecular events related to ion channel activation that are intractable using either conventional fluorescent-based probes or patch-clamp techniques.

Ion channels respond to various physical and chemical stimuli by regulating the flow of ions across the cell membranes. The resultant ion fluxes cause changes in cell membrane potential or alter intracellular ion concentrations, ultimately controlling cell responses. Ion flux regulation is, therefore, the main event by which ion channels trigger cell signaling. Anion/cation selectivity is a critical property of ion channels, underpinning their physiological function. Historically, ion selectivity was considered an immutable characteristic of an open ion channel, intrinsically determined by the structural organization of its constituent subunits. However, this uncompromising vision was challenged when dynamic changes in ion selectivity were measured during C-type inactivation of Kv channels, with an increase in channel permeability to sodium (1, 2). More recent studies demonstrated that, under acidic conditions or in low extracellular K^+ concentrations, the two-pore domain K^+ channel (K2P) TWIK1 exhibited dynamic changes in selectivity, becoming permeable to Na^+ and shifting from an inhibitory to an excitatory role (3–5). This phenomenon is responsible for the paradoxical depolarization of human cardiomyocytes in pathological hypokalemia, possibly contributing to cardiac arrhythmias. Dynamic ion selectivity may occur in other K2P channels, establishing a new regulatory mechanism for cell excitability (6).

Additionally, various studies have reported that the ion selectivity of P2X receptor channels and TRP ion channels, such as Transient Receptor Potential Vanilloid-1 Channel (TRPV1), may change dynamically in response to sustained agonist activation (7, 8) (reviewed in ref. 9). In the case of ligand-activated P2X and TRPV1 channels, it was even postulated that, if the pore initially opened rapidly to a conducting state that was relatively selective for small cations such as Na^+, K^+, and Ca^{2+}, the pore then gradually dilated over time to become more permeable to larger cations, such as fluorescent dyes or nonorganic ions (9–11). This phenomenon, known as "pore dilation," may elicit essential physiological functions and form the basis for therapeutic applications. Nonetheless, the study by Li et al. (12) seriously challenged the pore dilation theory based on the time-dependent ion selectivity change in P2X channels but did not question the permeability of gated P2X channels to large cations. These authors elegantly demonstrated that the time-dependent shift in the reversal potential (E_{rev}) measured in bi-ionic solutions was an artifact, warning about the results obtained when

Competing interest statement: Y.L.C., V.C., and Y.P. are co-inventors on a patent application related to the technology described in this article. All other authors declare no competing interests.

This article is a PNAS Direct Submission.

[1]To whom correspondence may be addressed. Email: yann.percherancier@ims-bordeaux.fr.

This article contains supporting information online at http://www.pnas.org/lookup/suppl/doi:10.1073/pnas.2205207119/-/DCSupplemental.

Published November 7, 2022.

measuring permeability changes during whole-cell patch-clamp recordings. Concomitantly, the study by Samways et al. (13) also presented convincing results casting doubts on time-dependent changes in the P_{Ca}/P_{Na} ratio during sustained activation of TRPV1 with capsaicin (CAPS) under voltage-clamp conditions (7, 8).

In the quest for compounds inducing a variation in ion selectivity in TRPV1, we found that AMG517, AMG21629, and BCTC, three well-known inhibitors of all TRPV1 activation modes (14), inhibited the CAPS-induced inward rather than the outward current but also induced a shift in E_{rev} in whole-cell patch-clamp experiments. To further characterize this effect, we took advantage of recently described resonance energy transfer (RET) sensors to measure the quantity of intracellular Ca^{2+} (15), K^+ (16), and ionic strength (17) in the vicinity of the TRPV1 pore in real time on live cells. These sensors were turned into bioluminescent resonance energy transfer (BRET) probes and fused to one extremity of the TRPV1 channel. The resulting BRET-based probes provided dynamic measurements of Ca^{2+} and K^+ concentrations and ionic strength in the nanoenvironment of the TRPV1 channel in real time and in live cells during drug challenges. Our results indicated that some TRPV1 antagonists displayed a differential potency in inhibiting CAPS-induced Ca^{2+} and K^+ fluxes. Even more strikingly, we found that AMG517 was a partial agonist of the K^+ efflux through TRPV1. In a further effort to exemplify ligand bias in other families of cationic channels, using the same BRET-based strategy, we also detected concentration- and time-dependent ligand biases in P2X7 and P2X5 cationic selectivity when activated by benzoylbenzoyl-adenosine triphosphate (Bz-ATP).

Results

Antagonist-Evoked Ionic Selectivity Changes in Capsaicin-Activated TRPV1 Measured Using Whole-Cell Automated Patch Clamp. We performed automated whole-cell patch-clamp experiments in HEK293T cells stably expressing TRPV1. As shown in Fig. 1, in the presence of 100 nM CAPS, the prototypic TRPV1 agonist, the TRPV1 current–voltage relationship (I/V curve) was outwardly rectifying. As expected, the subsequent application of a saturating concentration of either AMG517, BCTC, or AMG21629, three well-known TRPV1 antagonists (18, 19), decreased the magnitude of the current flow at both positive and negative voltages. Interestingly, in both conditions, the inward current was almost totally inhibited but not the outward current. In addition, both antagonists induced a leftward shift of the E_{rev}. The antagonist-induced variation in E_{rev} (ΔE_{rev}) was -21.2 ± 0.2, -20.8 ± 0.2, and -16.1 ± 0.3 mV, respectively, for AMG517, BCTC, and AMG21629. A further injection of a 10-fold more concentrated dose of the prototypic TRPV1 competitive antagonist capsazepine (CPZ) (20) partly reverted the AMG517/AMG21629 or BCTC-induced leftward shift in E_{rev} to a less negative value ($\Delta E_{rev} = +5 \pm 0.2$, $+4 \pm 0.2$, and $+4.2 \pm 0.3$ mV, respectively, for AMG517, BCTC, and AMG21629 (see *SI Appendix*, Fig. 1 for an enlarged view in the vicinity of the reversal potentials), and almost totally inhibited the remaining outward current, while the inward current stood close to the background level. These data suggested that AMG517, AMG21629, and BCTC, but not CPZ, preferentially inhibits the Ca^{2+}/Na^+ inward ion flux rather than the outward K^+ flux flowing through the gated TRPV1. These data inferred antagonist-dependent ion selectivity but required confirmation with an alternative technique. We, therefore, sought to develop TRPV1-based BRET probes capable of nanoscale measurement of cation concentration variations in the vicinity of the TRPV1 pore during gating.

Validation of the Fusion between TRPV1- and BRET-Based Calcium Biosensor for Measuring Calcium Influx in the Pore Nanoenvironment during Agonist-Promoted Gating. Since TRPV1 is known to be more selective for divalent than monovalent ion species, we started by measuring the intracellular Ca^{2+} rise in the TRPV1 pore nanoenvironment during gating. The human TRPV1 ion channel was thus fused to a slightly modified version of a recently described BRET sensor with a high affinity for calcium (Calflux-VTN) (15). We first sandwiched the troponin C domain (TnC) of the Calflux-VTN BRET sensor between the mNeonGreen (mNeonG) fluorescent and nano Luciferase (nanoLuc) (nLuc) bioluminescent proteins in both orientations, yielding two differently oriented BRET-based calcium sensors (mNeonG-Calflux-nanoLuc and nanoLuc-Calflux-mNeonG). Each BRET-based calcium sensor was then genetically fused to either the N- or C-terminal extremity of the human TRPV1 ion channel, yielding four different fusion proteins (Fig. 2*A* and *SI Appendix*, Fig. 2). Their functionality was assessed in the presence of increasing concentrations of CAPS following their transient expression in HEK293T cells. While a significant basal BRET signal was measured for each differently oriented construct, we observed that CAPS induced a concentration-dependent change in the basal BRET value for only three of them. There was no CAPS-induced BRET change when HEK293T cells were transfected with the nLuc-Calflux-mNeonG-TRPV1 BRET probe (*SI Appendix*, Fig. 2*B*). The greatest CAPS-induced BRET increase was measured using the mNeonG-Calflux-nLuc-TRPV1 fusion protein ($\Delta BRET_{max} = 1.32 \pm 0.03$, Fig. 2*A*). A very significant but less marked BRET change was also measured with both TRPV1-based BRET probes C-terminally fused to the Calflux sensor (*SI Appendix*, Fig. 2 *C* and *D*). This indicated that both the respective positions of the energy donor and acceptor in the Calflux BRET sensor, and the extremity of TRPV1 to which the sensor was fused, impacted the magnitude of the BRET change

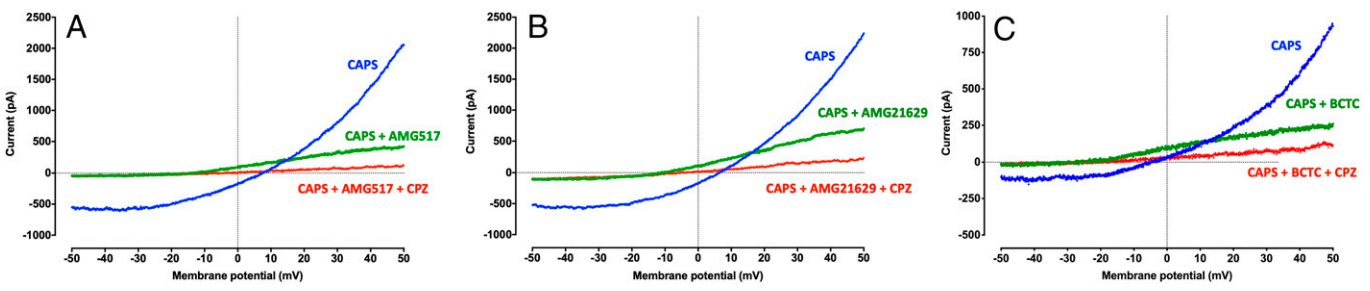

Fig. 1. Effect of AMG517, AMG21629, BCTC, and CPZ on CAPS-induced current in HEK cells stably expressing hTRPV1. I–V curves were obtained using automated patch-clamp assays in cells successively treated with 100 nM CAPS (blue curve), 1 μM AMG517 (*A*), 1 μM AMG21629 (*B*), or 1 μM BCTC (*C*) (green curve), and 10 μM CPZ (red curve). Data represent the average I/V curve of one out of three independent patched cells, with six to nine ramps performed per assay.

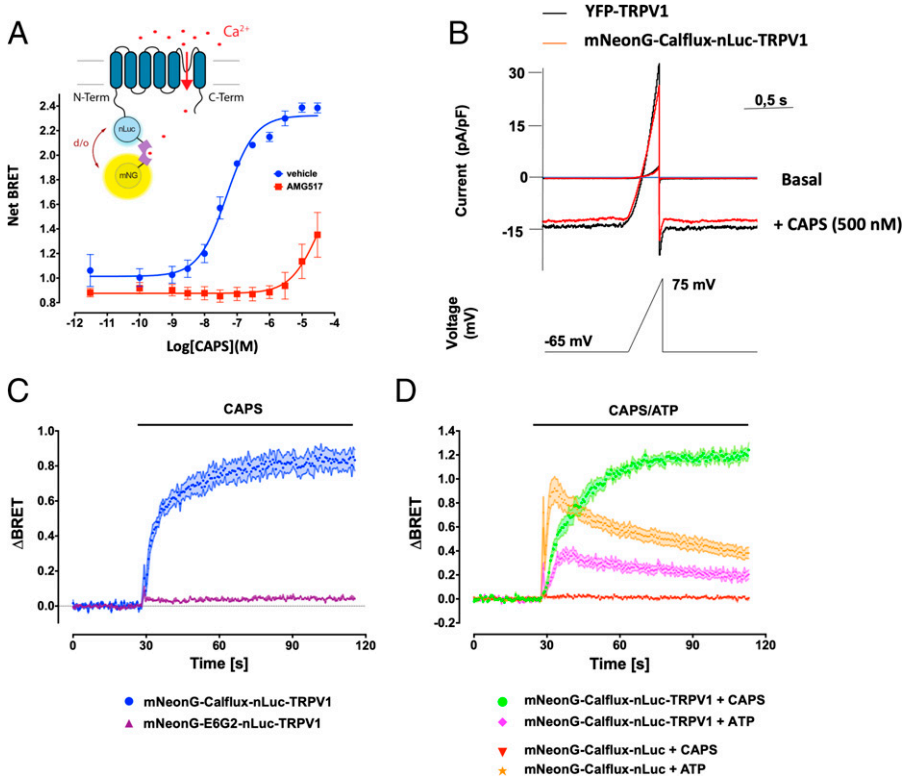

Fig. 2. Characterization of the mNeonG-Calflux-nLuc-TRPV1 probe. (*A*) Concentration–response curves of CAPS-induced BRET changes measured in HEK293T cells expressing the mNeonG-Calflux-nLuc-TRPV1 (n = 3). (*B*) Whole-cell current responses of HEK293T cells expressing YFP-TRPV1 (black line) and mNeonG-Calflux-nLuc-TRPV1 channels (red line) to a ramp voltage protocol from −65 mV to +75 mV (holding potential: −65 mV), in the presence or absence of CAPS (500 nM). (*C*) Kinetics of the CAPS (500 nM)-induced rise in the BRET signal in HEK293T cells transiently expressing either the mNeonG-Calflux-nLuc-TRPV1 (n = 8) or mNeonG-E6G2-nLuc-TRPV1 BRET probe (n = 8). (*D*) Kinetics of the CAPS (10 μM) or ATP (100 μM)-induced rise in the BRET signal in HEK293T cells transiently expressing either the unfused mNeonG-Calflux-nLuc BRET or the mNeonG-Calflux-nLuc-TRPV1 BRET probe (n = 6 to 10 depending on the condition).

measured during TRPV1 gating. The pharmacological selectivity of the ligand-promoted BRET changes measured was further demonstrated by the right shift of the half-maximal response of each TRPV1-based BRET probe in the presence of AMG517 (Fig. 2 and *SI Appendix*, Fig. 2).

Since the largest CAPS-induced BRET variation was obtained using the mNeonG-Calflux-nLuc-TRPV1 BRET probe, this configuration was chosen for the rest of the study. Similar to our findings with earlier intra- and intermolecular TRPV1-based BRET probes sensing TRPV1 conformational changes and calmodulin (CaM) coupling during gating (21, 22), we showed that CAPS increased the mNeonG-Calflux-nLuc-TRPV1 basal BRET with first-order kinetics (Fig. 2 *C* and *D*) and potency (pEC_{50} = 7.32 ± 0.08, Fig. 2*A*) matching the values reported in the literature (23, 24). However, the magnitude of the largest BRET variation measured with the mNeonG-Calflux-nLuc-TRPV1 BRET probe was at least fivefold higher than those measured with the intra- and intermolecular TRPV1-based BRET probes (*SI Appendix*, Fig. 2*E*), thus highlighting the potential of these BRET probes. Several verifications were nonetheless required before accepting the mNeonG-Calflux-nLuc-TRPV1 BRET probe as a tool for TRPV1 ion channel studies.

Firstly, we verified that the CAPS-induced whole-cell current was of similar magnitude in HEK293T cells expressing either YFP-TRPV1 or mNeonG-Calflux-nLuc-TRPV1 (Fig. 2*B*), knowing that N-terminal YFP fusion does not alter TRPV1 permeability to Ca^{2+} (21, 25). These results indicated, therefore, that the N-terminal fusion of the mNeonG-Calflux-nLuc BRET sensor to TRPV1 did not alter its electrophysiological properties.

Secondly, it was necessary to determine that the BRET variation measured with this probe during TRPV1 gating was not caused by changes in the various modes of energy transfer between nLuc and mNeonG inside the tetrameric organization of TRPV1 during channel opening (21, 25). To verify this hypothesis, we replaced the calcium-sensitive Calflux sequence in our TRPV1-based BRET probe with the E6G2 sequence, which senses macromolecular crowding (26), yielding the mNeonG-E6G2-nLuc-TRPV1 BRET probe. As shown in Fig. 2*C*, following CAPS activation, no BRET increase was measured in HEK293T cells transfected with this probe. This indicated that the BRET variation measured using the mNeonG-Calflux-nLuc-TRPV1 BRET probe was caused by the increase in Ca^{2+} concentration in the intracellular vicinity of the TRPV1 pore rather than conformational changes in the quaternary structure of the TRPV1 ion channel during gating.

Finally, it was essential to verify that the BRET variation measured using the mNeonG-Calflux-nLuc-TRPV1 probe did not result in Ca^{2+} influx through an off target. To control for this experimental bias, we took advantage of the endogenous expression of P2Y purinergic receptors in HEK293T cells (27). HEK293T cells transiently transfected with the unfused mNeonG-Calflux-nLuc or mNeonG-Calflux-nLuc-TRPV1 BRET probes were challenged with either CAPS or ATP. As expected, CAPS did not trigger any BRET increase in the HEK293T cells transfected with the mNeonG-Calflux-nLuc BRET probe alone, but induced a rapid, sustained BRET increase in HEK293T cells transiently transfected with the mNeonG-Calflux-nLuc-TRPV1 BRET probe (Fig. 2*D*). In contrast, ATP caused an immediate, robust increase in the soluble mNeonG-Calflux-nLuc BRET ratio that decreased rapidly over time (Fig. 2*D*), as expected for the P2Y response to ATP (28). Finally, ATP only induced a low-magnitude, transient increase in the mNeonG-Calflux-nLuc-TRPV1 BRET probe signal. Knowing that extracellular ATP is a well-known TRPV1 sensitizer, part of this signal could be due to TRPV1 direct activation at 37 °C (27). Altogether, these results indicate that, if any other sources of intracellular calcium increase contributed to the BRET signal, their impact was minimal.

Measuring Intracellular Variations in Potassium and Monovalent Ionic Strength in the TRPV1 Pore Nanoenvironment during Agonist-Promoted Gating. Knowing that TRPV1 is a nonselective cation channel, the next step was to use the same molecular

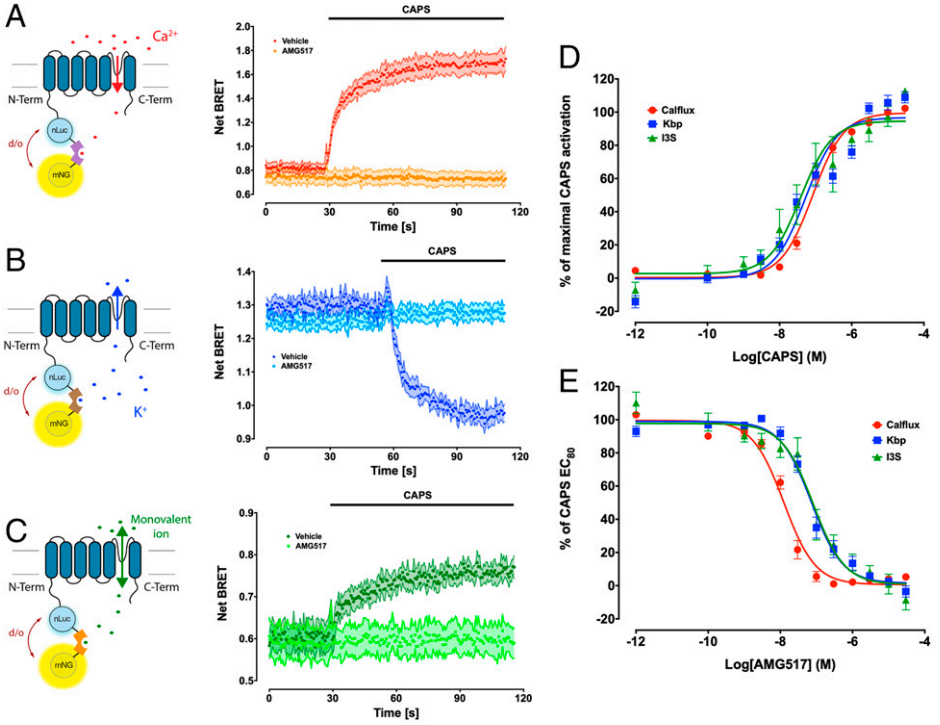

Fig. 3. (*A–C*) Schematic representations (*Left*) and kinetic of the CAPS (500 nM)-induced change in the BRET signal (*Right*) measured with mNeonG-Calflux-nLuc-TRPV1 (*A*, *n* = 10), mNeonG-Kbp-nLuc-TRPV1 (*B*, *n* = 11), or mNeonG-I3S-nLuc-TRPV1 (*C*, *n* = 6) BRET probes. AMG517 (10 μM) or vehicle was preincubated for 5 min before adding CAPS to the culture medium. (*D*) Concentration–response curves of CAPS-induced BRET changes measured in HEK293T cells transiently expressing the mNeonG-Calflux-nLuc-TRPV1 (*n* = 13), mNeonG-Kbp-nLuc-TRPV1 (*n* = 13), or mNeonG-I3S-nLuc-TRPV1 (*n* = 6) BRET probes. (*E*) Concentration–response curves of the ability of AMG517 to inhibit CAPS (500 nM)-induced BRET changes in HEK293T cells expressing the mNeonG-Calflux-nLuc-TRPV1 (*n* = 13), mNeonG-Kbp-nLuc-TRPV1 (*n* = 13), or mNeonG-I3S-nLuc-TRPV1 (*n* = 6) BRET probes.

strategy to measure dynamic variations in TRPV1 permeability to other cations during gating. To measure TRPV1 permeability to K^+ during gating, we used the recently described K^+-sensitive genetically encoded Förster resonance energy transfer (FRET)-based probe, developed to measure K^+ dynamics in real time (K^+-binding protein [Kbp] sensor) (16). However, designing a Na^+-sensitive BRET probe was problematic since, to our knowledge, no sodium-binding protein with an affinity in the nanomolar range has yet been described. We were, however, able to build on a recently described ionic-strength FRET biosensor that relies on a positively and a negatively charged α-helix, with electrostatic attraction dependent on local ionic strength of monovalent ions (17). Following the same strategy used with the Calflux-VTN BRET probe (Fig. 3 *A*, *Left*), we sandwiched both the K^+-binding protein (Kbp) described by Bischof et al. (16), and the ionic strength sensitive sequence (hereafter called I3S), described by Liu et al. (17), between the mNeonG fluorescent acceptor at their N-terminal extremities and the nanoLuc bioluminescent donor at their C-terminal extremities. The resulting mNeonG-Kbp-nLuc and mNeonG-I3S-nanoLuc BRET sensors were then N-terminally fused to TRPV1, yielding the mNeonG-Kbp-nLuc-TRPV1 (Fig. 3 *B*, *Left*) and mNeonG-I3S-nLuc-TRPV1 BRET probes (Fig. 3 *C*, *Left*).

HEK293T cells expressing each of these BRET probes were then processed separately for BRET analysis. In both cases, the basal BRET, measured under resting conditions, varied with first-order kinetics after exposure to CAPS (Fig. 3), as already shown for the mNeonG-Calflux-nLuc-TRPV1 probe (Figs. 2*C* and 3 *A*, *Right*) and our former TRPV1-based intra- and intermolecular BRET probes (21). However, the addition of CAPS induced a decrease in basal BRET with the mNeonG-Kbp-nLuc-TRPV1 probe and an increase in basal BRET with mNeonG-I3S-nLuc-TRPV1 (Fig. 3 *B* and *C*, *Right*). Knowing that the efficiency of resonant energy transfer between the donor and acceptor groups encompassing the Kbp sensor increased with the concentration of K^+ ions (16), while the resonant energy transfer efficiency between the donor and acceptor groups encompassing the I3S sensor decreased as the environmental ionic strength increased (17), our results indicated that both intracellular K^+ and ionic strength of monovalent ions decreased when Ca^{2+} increased in the nanoenvironment of the TRPV1 pore following CAPS-induced TRPV1 gating. These effects were completely abolished in cells preincubated with AMG517, thereby highlighting the specificity of the assays.

Remarkably, a dose–response analysis revealed that, while CAPS potency to activate TRPV1 was almost identical for all BRET probes (Fig. 3*D*), the AMG517 potency to inhibit CAPS-induced TRPV1 activation was right shifted by almost one log for both the mNeonG-Kbp-nLuc-TRPV1 and mNeonG-I3S-nLuc-TRPV1 probes in comparison with mNeonG-Calflux-nLuc-TRPV1 (Fig. 3*E*, see also Table 1).

Since the I3S probe is mainly insensitive to Ca^{2+} (17), our data thus suggested that, under physiological conditions, 1) the K^+ efflux may overcome the Na^+ influx in response to CAPS-induced TRPV1 gating, and 2) AMG517 may differentially inhibit both Ca^{2+} and K^+ fluxes through the open TRPV1 pore.

Assessment of the Cross-Talk between the K^+ Efflux and the Na^+/Ca^{2+} Extracellular Ions. As stated in a very comprehensive review by Cao (29): "Ion selectivity of TRP channels is perhaps defined by interaction energy of competing permeable cations with dynamic selectivity filters, which is beyond what can be gleaned from only inspecting the existing static snapshots of TRP channel structures." The advent of BRET probes suited for assessing the dynamics of various cytoplasmic cations in the TRPV1 pore nanoenvironment thus offered the opportunity to study the dynamic interplay among cations to access the TRPV1 pore.

TRPV1 being more specific for Ca^{2+} than for K^+ or Na^+ (7, 23), we challenged HEK293T cells expressing either mNeonG-Calflux-nLuc-TRPV1 (Fig. 4*A*) or the mNeonG-Kbp-nLuc-TRPV1 probe (Fig. 4*B*) with increasing concentrations of CAPS in the presence or absence of extracellular Ca^{2+}. The basal

Table 1. pEC_{50}/pIC_{50} values derived from curve fitting TRPV1 agonist/antagonist dose–responses, measured using either the mNeonG-Calflux-nLuc-TRPV1 or mNeonG-Kbp-nLuc-TRPV1 BRET probes

		mNeonG-Calflux-nLuc-TRPV1	mNeonG-Kbp-nLuc-TRPV1	*P* value
Agonists	Capsaicin	7.08 ± 0.03 (13)	7.13 ± 0.04 (13)	n.s.
	Olvanil	6.53 ± 0.06 (8)	6.96 ± 0.09 (8)	*
	RTX	8.30 ± 0.05 (9)	8.11 ± 0.06 (9)	n.s.
Antagonists	AMG517	7.90 ± 0.04 (13)	7.14 ± 0.06 (13)	****
	BCTC	8.10 ± 0.12 (5)	7.35 ± 0.10 (5)	**
	AMG21629	8.46 ± 0.07 (7)	7.85 ± 0.07 (7)	***
	CPZ	5.76 ± 0.08 (7)	5.71 ± 0.08 (7)	n.s.
	JNJ17203212	6.84 ± 0.09 (6)	6.65 ± 0.12 (6)	n.s.
	AMG9810	6.39 ± 0.13 (6)	5.74 ± 0.11 (6)	*

Values represent the mean ± SE of (*n*) independent experiments performed in duplicate. n.s., not significant; *$P < 0.05$; **$P < 0.01$; ***$P < 0.001$; ****$P < 0.0001$.

BRET ratio of the calcium-sensing TRPV1-based BRET probe increased slightly in the absence of extracellular Ca^{2+}. The reason for this is not clear, but it may indicate that, in the absence of extracellular Ca^{2+}, more Ca^{2+} may be released from internal stores in the cytosol. However, as expected, removal of extracellular Ca^{2+} almost completely abolished CAPS-induced calcium influx. In parallel, chelation of extracellular Ca^{2+} induced a ∼75% decrease in the basal BRET ratio measured in HEK293T cells transfected with the mNeonG-Kbp-nLuc-TRPV1 probe (Fig. 4 *B* and *C*). Intriguingly, in the absence of extracellular Ca^{2+}, CAPS still induced a dose-dependent decrease in K^+ in the nanoenvironment of the TRPV1 pore (Fig. 4 *B* and *C*), which was characterized by a small leftward shift of the CAPS potency (pEC_{50} = 8.01 ± 0.3 in the presence of Ca^{2+} vs. 8.54 ± 0.37 in the presence of aminopolycarboxylic acid (EGTA), $n = 8$, $P < 0.05$), and a slightly lower plateau at high CAPS concentrations (Fig. 4*B*). Such results suggested either that there is a competitive cation interaction between K^+ and Ca^{2+} or that removing Ca^{2+} lifts Ca^{2+}-dependent TRPV1 desensitization under the experimental conditions studied (i.e., 37 °C). Since Ba^{2+} does not support TRPV1 desensitization (30), we therefore substituted Ba^{2+} for Ca^{2+}. As expected, in the presence of extracellular Ba^{2+}, CAPS only slightly increased the BRET signal measured in cells expressing the mNeonG-Calflux-nLuc-TRPV1 (Fig. 4*A*). However, Ca^{2+} replacement by Ba^{2+} did not trigger any K^+ efflux (Fig. 4*B*), and the basal concentration of K^+ was even slightly increased. As a result, there was an offset in the concentration–response curve for CAPS to higher BRET values, but with no change in CAPS potency to trigger the K^+ efflux. Importantly, AMG517 completely abolished the K^+ efflux measured in the presence of EGTA (Fig. 4*C*). Taken together, these data argue much more in favor of a competition between K^+ and Ca^{2+} for accessing the TRPV1 pore than a desensitization lift leading to K^+ efflux, which should also have occurred in the presence of Ba^{2+}.

Interestingly, the absence of extracellular Ca^{2+} decreased the intracellular monomeric ionic strength near the TRPV1 pore similarly to CAPS, as measured by the increase in BRET signal with the mNeonG-I3S-nLuc-TRPV1 BRET probe (Fig. 4*D*). However, no additive effect of CAPS and EGTA was observed. Finally, in agreement with the studies by Ohta et al. and Jara-Oseguera et al. (31, 32) showing that Na^+ negatively regulates the gating and polymodal sensitization of the TRPV1 channel, we found that replacement of extracellular Na^+ by the large monovalent cation *N*-methyl-D-glucamine ($NMDG^+$) both increased the basal intracellular Ca^{2+} concentration in the vicinity of the TRPV1 pore and left shifted the CAPS potency to trigger a Ca^{2+} influx (*SI Appendix*, Fig. 3). This effect was accompanied by a concomitant slight increase in the K^+ basal level in the pore nanoenvironment without any shift in CAPS potency to trigger a K^+ efflux through TRPV1. Whether this reflects a balance between lifting of the Na^+ negative effect on K^+ efflux and increased competition with Ca^{2+} influx remains to be determined.

In order to confirm these results, we assessed the effect of Ca^{2+} removal on K^+ efflux through TRPV1 using whole-cell voltage clamp. Using physiological concentrations of external Na^+ ($[Na^+]_{out}$) and Ca^{2+} ($[Ca^{2+}]_{out}$), and K^+ as the main internal cation ($[K^+]_{int}$), removing $[Ca^{2+}]_{out}$ (by introduction of EGTA [500 μM] into the bath) repeatedly increased the outward K^+ flux at positive potential (*SI Appendix*, Fig. 4*A*) but also at negative potential close to the HEK293T plasma membrane resting potential (E_m) (*SI Appendix*, Fig. 4*B*, see also *SI Appendix*, Table 2). EGTA was unable to produce such an effect on untransfected HEK293T cells (*SI Appendix*, Fig. 4*C*). Moreover, using a current-clamp technique with $NMDG^+$ and Ca^{2+} as the external cations, and K^+ as the only internal cation, EGTA clearly hyperpolarized the cell membrane (*SI Appendix*, Fig. 4*D*), indicating that in our experimental conditions, the removal of $[Ca^{2+}]_{out}$ effectively triggered an outflow of $[K^+]_{int}$. In this last experiment, $[Na^+]_{out}$ was substituted by $[NMDG^+]_{out}$ to lift the TRPV1 inhibition by Na^+ (31, 32) and to better assess the potassic current, as this is the only one measured with the mNeon-Kbp-nLuc-TRPV1 BRET probe. In addition, the current–voltage relation obtained in the presence of CAPS showed outward rectification whether $[Ca^{2+}]_{out}$ was present or not (*SI Appendix*, Fig. 4*E*). However, while the K^+ outward current measured at positive potential was almost unchanged by $[Ca^{2+}]_{out}$ removal, the Na^+ inward current measured at negative potential was of very low intensity. Importantly, the E_{rev}, which was measured at −0.51 ± 1.01 mV ($n = 7$) in the presence of CAPS and $[Ca^{2+}]_{out}$, was shifted to −19.3 ± 1.19 mV ($n = 3$) when CAPS and EGTA were introduced together into the bath (*SI Appendix*, Fig. 4*E*). These data confirmed that, as shown with our BRET probes (Fig. 4), in the absence of $[Ca^{2+}]_{out}$, the K^+ efflux is effectively much more increased through the CAPS-gated TRPV1 than the residual Na^+ influx.

Comparison of the Selective Triggering or Inhibition of Ca^{2+} or K^+ Fluxes through TRPV1 by Reference Compounds. We then aimed at assessing whether other ligands also differentially modulated TRPV1 permeability to Ca^{2+} and K^+. Concentration–response curves in HEK293T cells expressing either the mNeonG-Calflux-nLuc-TRPV1 or mNeonG-Kbp-nLuc-TRPV1 BRET probes revealed that, as observed with CAPS, resiniferatoxin (RTX) displayed similar potencies to trigger Ca^{2+} influx and K^+ efflux (Fig. 5*A* and Table 1). Olvanil was however slightly more potent to trigger the K^+ efflux than the Ca^{2+} influx (Fig. 5*B* and Table 1).

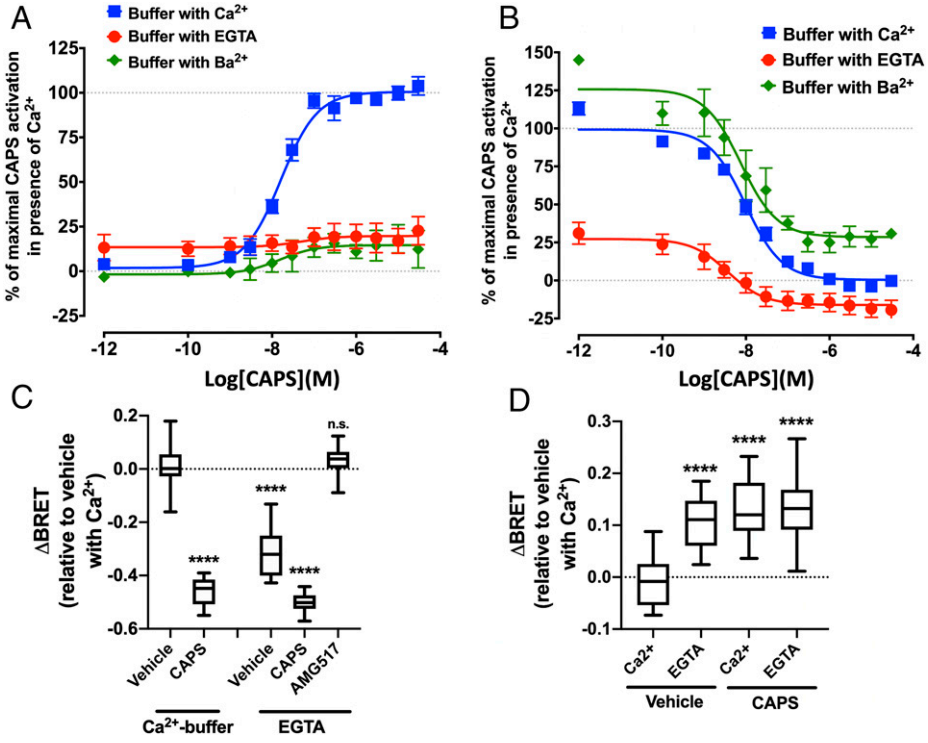

Fig. 4. (*A* and *B*) Concentration–response curves of CAPS-induced BRET changes in HEK293T cells expressing either the mNeonG-Calflux-nLuc-TRPV1 (*A*) or mNeonG-Kbp-nLuc-TRPV1 probe (*B*), in the presence or absence of extracellular Ca^{2+} or following the substitution of Ba^{2+} for Ca^{2+}. (*C* and *D*) Box and whisker plots representing the mixed impact of calcium deprivation (EGTA), CAPS (500 nM), and AMG517 (10 μM) on the basal BRET measured in the presence of extracellular Ca^{2+} in untreated HEK293T cells that were either transfected with the mNeonG-Kbp-nLuc-TRPV1 (*C*, $n = 16$) or mNeonG-I3S-nLuc-TRPV1 (*D*, $n = 18$) BRET probes. When present, the external concentration of Ba^{2+} and Ca^{2+} was 1 mM. For assays performed in the absence of Ca^{2+}, cells were washed once with a buffer without Ca^{2+} and EGTA 2 mM (w/o Ca^{2+}/with EGTA) before the assay was performed in the same fresh buffer. Results represent the variation in basal BRET between the control condition and the various treatments. Statistical significance of the derivation from the null hypothesis (no difference between control condition [vehicle in presence of Ca^{2+}] and one treated condition) was assessed using the one-sample Wilcoxon signed-rank test. n.s., not significant; ****$P < 0.0001$.

Of note, the rank order of EC_{50} and maximal efficacy values for each agonist was the same for the two BRET biosensors with RTX > CAPS > olvanil (*SI Appendix*, Fig. 5). While these results are in full agreement with the literature concerning the agonist-induced TRPV1 permeability to Ca^{2+} (33–35), our study extends this observation to the agonist-induced TRPV1 permeability to K^+ and suggests that the balance of ion fluxes through TRPV1 is intrinsically dependent upon the agonist used.

Considering the TRPV1 antagonists, in addition to AMG517, the compounds AMG21629, AMG9810, and BCTC, also displayed a higher potency to inhibit the Ca^{2+} influx than the K^+ efflux, both triggered by an EC_{80} of CAPS (Fig. 5 *C–E* and Table 1). Neither of the two other antagonists tested (CPZ and JNJ17203212) caused such a ligand bias (Fig. 5 *F* and *G* and Table 1). These findings indicated that some known TRPV1 antagonists exert ion-specific inhibition of the CAPS-induced Ca^{2+} and K^+ fluxes through TRPV1.

Knowing that a partial agonist partly antagonizes the activity of a full agonist, these compounds, therefore, behave either as pure antagonists or as partial agonists of each flux but with different potencies. To distinguish between these possibilities, kinetic experiments were performed in HEK293T cells expressing either the mNeonG-Calflux-nLuc-TRPV1 or mNeonG-Kbp-nLuc-TRPV1 BRET probes in the presence of AMG517, BCTC, CPZ, and AMG21629. As shown in Fig. 6*A*, while an EC_{80} of CAPS induced a robust, sustained increase in the BRET ratio in cells expressing the mNeonG-Calflux-nLuc-TRPV1 BRET probe, BCTC and AMG517 induced only a very transient, slight amplitude increase in the intracellular Ca^{2+} concentration in the vicinity of the TRPV1 channel pore. The reason for this intracellular calcium puff is not clear. It may be related to the complete expulsion of Ca^{2+} trapped in either the outer pore entrance or central pore vestibule during antagonist-driven conformational changes leading to a less Ca^{2+}-permeable TRPV1 conformation. Such transient calcium increase was almost undetectable when CPZ or AMG21629 was used. All antagonists efficiently blocked the CAPS-induced BRET increase.

Strikingly, AMG517 triggered a sustained K^+ decrease, ∼30% of the one triggered by CAPS (Fig. 6*B*). BCTC only triggered a transient and less marked K^+ decrease. No similar effect was measured using CPZ and AMG21629, as injection did not modify the BRET signal baseline measured with the mNeonG-Kbp-nLuc-TRPV1 BRET probe. Altogether, these results are in agreement with the notion that AMG517, BCTC, and AMG21629 are authentic, potent antagonists of the Ca^{2+} flux (36, 37). At the same time, AMG517, but not AMG21629, behaves as a weak partial agonist of the K^+ flux. BCTC only induced a very transient, slight amplitude efflux of K^+ paralleling the kinetic of the calcium puff, making it difficult to categorize. As expected, CPZ behaved as a pure antagonist of both Ca^{2+} and K^+ fluxes.

Knowing that potassium is the dominant ion controlling resting membrane potential (38), potassium efflux through the biased opening of the TRPV1 channel, even at low levels, may induce hyperpolarization. As this event depends on the potassium ion's driving force, and since the Nernst potential for the potassium ion is about −90 mV, it only occurs in relatively depolarized cells. Knowing that the membrane potential of HEK293T cells is around −25 mV (39), we tested whether AMG517 differentially modulated the membrane potential of these cells when transiently expressing TRPV1. As expected, CAPS induced membrane depolarization of HEK293T cells transfected with TRPV1, as indicated by a net increase in the signal measured using a fluorometric membrane potential dye (Fig. 6*C*). In sharp contrast, among all the antagonists tested, only AMG517 induced a time-dependent signal decrease with a time constant similar to that measured in the presence of CAPS in TRPV1-expressing HEK293T cells (Fig. 6*C*) but not in untransfected HEK293T cells (*SI Appendix*, Fig. 6 *A* and *B*). We confirmed the effect of AMG517 on ramp depolarization and membrane potential measured in HEK293T cells transiently expressing YFP-TRPV1, and using the $[NMDG^+]_{out}/[Ca^{2+}]_{out}$ and $[K^+]_{int}$ experimental condition. As shown in *SI Appendix*, Fig. 6*C*, AMG517 increased the potassic outward current at positive potential and at −30 mV, close to the resting

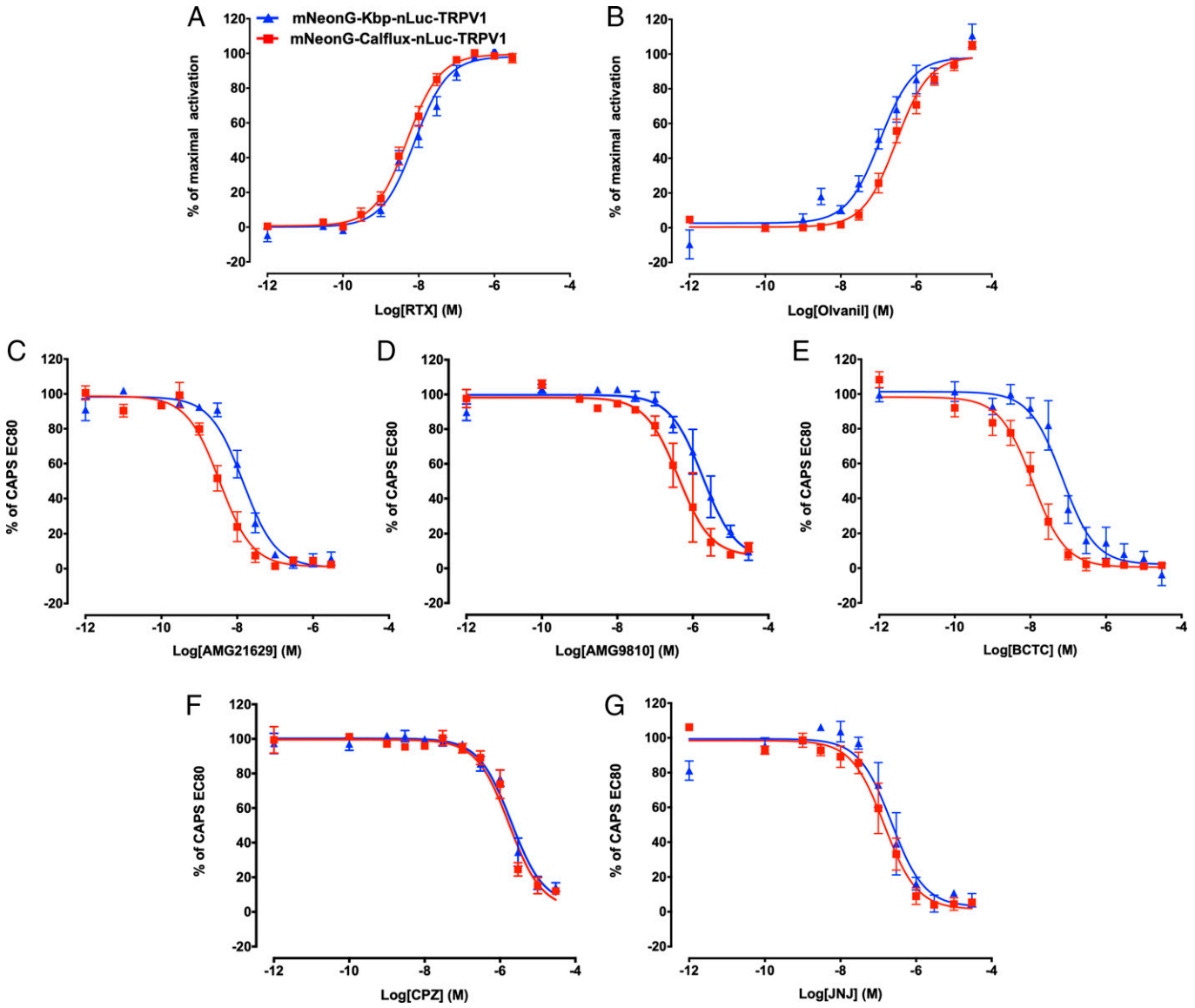

Fig. 5. (*A* and *B*) Variations in the BRET signal measured in HEK293T cells expressing either the mNeonG-Calflux-nLuc-TRPV1 (red curves) or mNeonG-Kbp-nLuc-TRPV1 BRET probes (blue curves) in response to increasing quantities of RTX (*A*) or olvanil (*B*). (*C*–*G*) Concentration–response curves of the ability of AMG21629 (*C*), AMG9810 (*D*), BCTC (*E*), CPZ (*F*), and JNJ17203212 (*G*), to inhibit CAPS (500 nM)-induced BRET changes in HEK293T cells expressing the mNeonG-Calflux-nLuc-TRPV1 (red curves) or mNeonG-Kbp-nLuc-TRPV1 (blue curve) BRET probes. The calculated EC_{50}/IC_{50} and number of replicates are indicated in Table 1.

membrane potential of the HEK293T cells (*SI Appendix*, Table 2). Finally, the impact of AMG517 on TRPV1 was further confirmed by current-clamp experiment showing that AMG517 reversibly hyperpolarized the cells' membrane potential (*SI Appendix*, Fig. 6*D*).

Measuring Intracellular Calcium and Potassium Concentrations in the Vicinity of the P2X Ligand-Gated Ion Channel Pore. We next tested whether our ionic BRET sensors could also monitor ion flux through ligand-gated ion channels, such as P2X purinergic receptors. We, therefore, fused the mNeonG-Calflux-nLuc sensor to the C-terminal tails of the seven human P2X subunits (Fig. 7*A*). Among the seven probes, time- and concentration-dependent ATP increases in BRET signals were observed for P2X2 (Fig. 7 *B*, *Left*) and P2X4 (Fig. 7 *B*, *Right* and Fig. 7*C*). Similar observations were made for P2X5 (Fig. 7*C*). In the case of P2X4, slow desensitization of the receptor was observed following prolonged ATP application, as already described (40). Because of the rapid desensitization of P2X1 and P2X3 receptors and the inability of P2X6 subunits to generate functional homomeric receptors, we did not characterize in detail the BRET probes for these three subunits. The apparent potencies (pEC_{50}) of ATP to trigger an influx of Ca^{2+} for the others P2X subunits are given in *SI Appendix*, Table 1.

In the next experiment, K^+ permeability through the P2X receptor pores was monitored by fusing the mNeonG-Kbp-nLuc sensor to the C-terminal tail of the human P2X subunits (Fig. 7*D*). We aimed at comparing over time Ca^{2+} and K^+ permeability changes of hP2X7, a receptor that undergoes a facilitation phenomenon (41) and which is associated with an apparent pore dilation. Benzoyl ester of ATP (Bz-ATP), which is by far the most potent P2X7 agonist, was used to activate the receptor. A similar analysis was performed on hP2X5, another P2X receptor activated by Bz-ATP. Time- and dose-dependent Bz-ATP decreases in BRET were observed in these two receptors (Fig. 7 *E* and *G*, *Right*), confirming that hP2X-mNeonG-Kbp-nLuc probes were able to track the potassium permeability of these two receptors. The BRET variation in Ca^{2+}- and K^+-sensitive probes during the

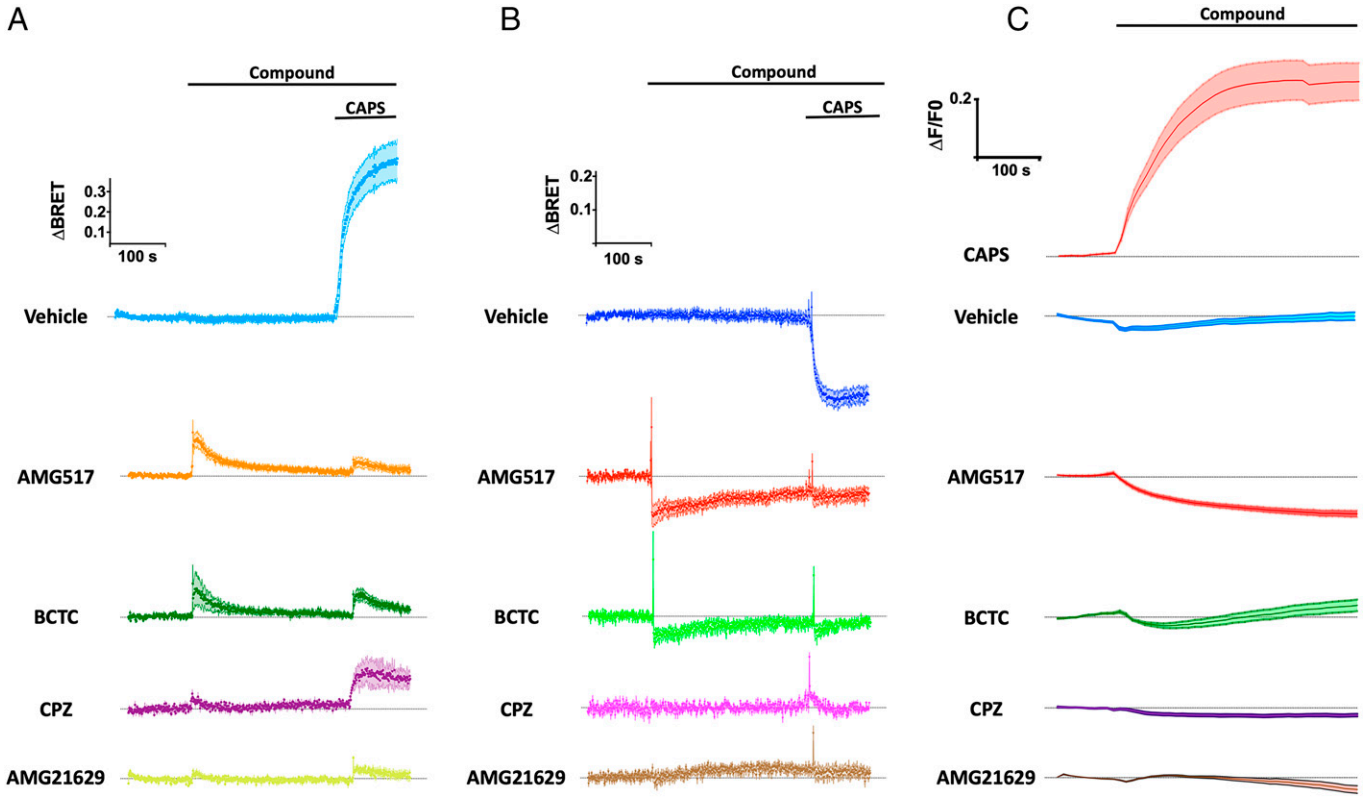

Fig. 6. Kinetics of the effect of vehicle (n = 14), AMG517 (10 μM, n = 12), BCTC (10 μM, n = 7), CPZ (10 μM, n = 4), and AMG21629 (1 μM, n = 6) on the basal BRET measured in HEK293T cells transiently expressing either mNeonG-Calflux-nLuc-TRPV1 (*A*) or mNeonG-Kbp-nLuc-TRPV1 (*B*). CAPS (500 nM) was injected when indicated. (*C*) Kinetics of the effect of CAPS (500 nM, n = 6), vehicle (n = 6), AMG517 (10 μM, n = 6), BCTC (10 μM, n = 5), CPZ (10 μM, n = 4), or AMG21629 (1 μM, n = 3) on the membrane potential of HEK293T cells transiently transfected with TRPV1.

first 3 min after Bz-ATP injection indicated that Bz-ATP had a similar potency to induce Ca^{2+} influx and K^+ efflux through P2X5 (Fig. 7 *F* and *G*, and *SI Appendix*, Table 1). The potency of Bz-ATP to trigger Ca^{2+} influx through P2X7 during the same period, however, was slightly higher than its potency to induce K^+ efflux through P2X7 (Fig. 7 *E* and *F* and *SI Appendix*, Table 1).

Moreover, the time-dependent relative permeability of P2X5 and P2X7 to Ca^{2+} and K^+ changed over time following the Bz-ATP challenge (Fig. 7*H*). In both P2X5 and P2X7, Bz-ATP triggered an immediate Ca^{2+} rise that decreased slightly after peaking. In sharp contrast, K^+ never peaked but increased slowly over time following Bz-ATP addition to the cell culture medium (Fig. 7 *E* and *G*). This phenomenon was exacerbated at the highest Bz-ATP concentration tested (1 mM) on P2X5. While the permeability of P2X5 to calcium was highest 1 min after Bz-ATP injection, it then dropped dramatically to a level close to the background. At the same time, permeability to K^+ increased gradually and was maintained over time. Taken together, these results confirmed that our ionic BRET biosensors were effective at monitoring ligand-gated ion-channel activation and represent valuable tools for tracking specific ion permeability during receptor gating.

Discussion

Tracking selective ion permeability through ion channels is challenging. To date, the only way to study specific ionic flux during ion channel gating has been electrophysiological recording. Using this technique, intra- or extracellular media must be constrained during electrophysiological recording, therefore precluding the monitoring of ion flux under physiological conditions and leading to technical bias such as the phenomenon of "ion accumulation" (12, 13). In this work, we generated highly sensitive BRET probes for real-time, noninvasive measurement of specific ion concentration changes in the vicinity of TRPV1 and P2X pores in live cells.

Our BRET study on TRPV1 produced three significant results. Firstly, while all tested agonists, except olvanil, displayed equivalent potency to gate the TRPV1 channel for both Ca^{2+} and K^+, among the antagonists tested, AMG517, AMG21629, and BCTC were more potent in inhibiting CAPS-induced Ca^{2+} influx than CAPS-induced K^+ efflux. Secondly, we found that AMG517, but not BCTC or AMG21629, was a long-lasting partial agonist of K^+ efflux through TRPV1. Thirdly, AMG517 induced TRPV1-dependent hyperpolarization of HEK293T cells. These results indicate that antagonists display biased activity when interacting with a given ion channel by selectively and differentially modulating the flux of different ions through the gated channel.

Which hypotheses may explain ligand bias on TRPV1 on a structural level? It is known that the pore regions of TRPV1/2/3/4 exhibit significant sequence homology with the selectivity filter of the bacterial K^+ ion channel (KcsA). This includes the signature sequence motif T*X*GYGD—T*X*GMGD in TRPV1 channels—that suggests a similar pore organization (42). Furthermore, at the outermost site of their selectivity filter facing the extracellular vestibule, most TRP channels contain a negatively charged residue, predominantly aspartic acid. The mutation of this amino acid has been shown to affect ion selectivity (reviewed in ref. 29). Interestingly, point mutation of the human TRPV1 selectivity filter at position D646 and the corresponding mutation of murine TRPV4 at position D682 have been shown to reduce permeability to Ca^{2+} (43, 44), thus rendering both ion channels selective for monovalent ions. While the amino acid at this position may not account for all the pore properties, suggesting the existence of additional structural

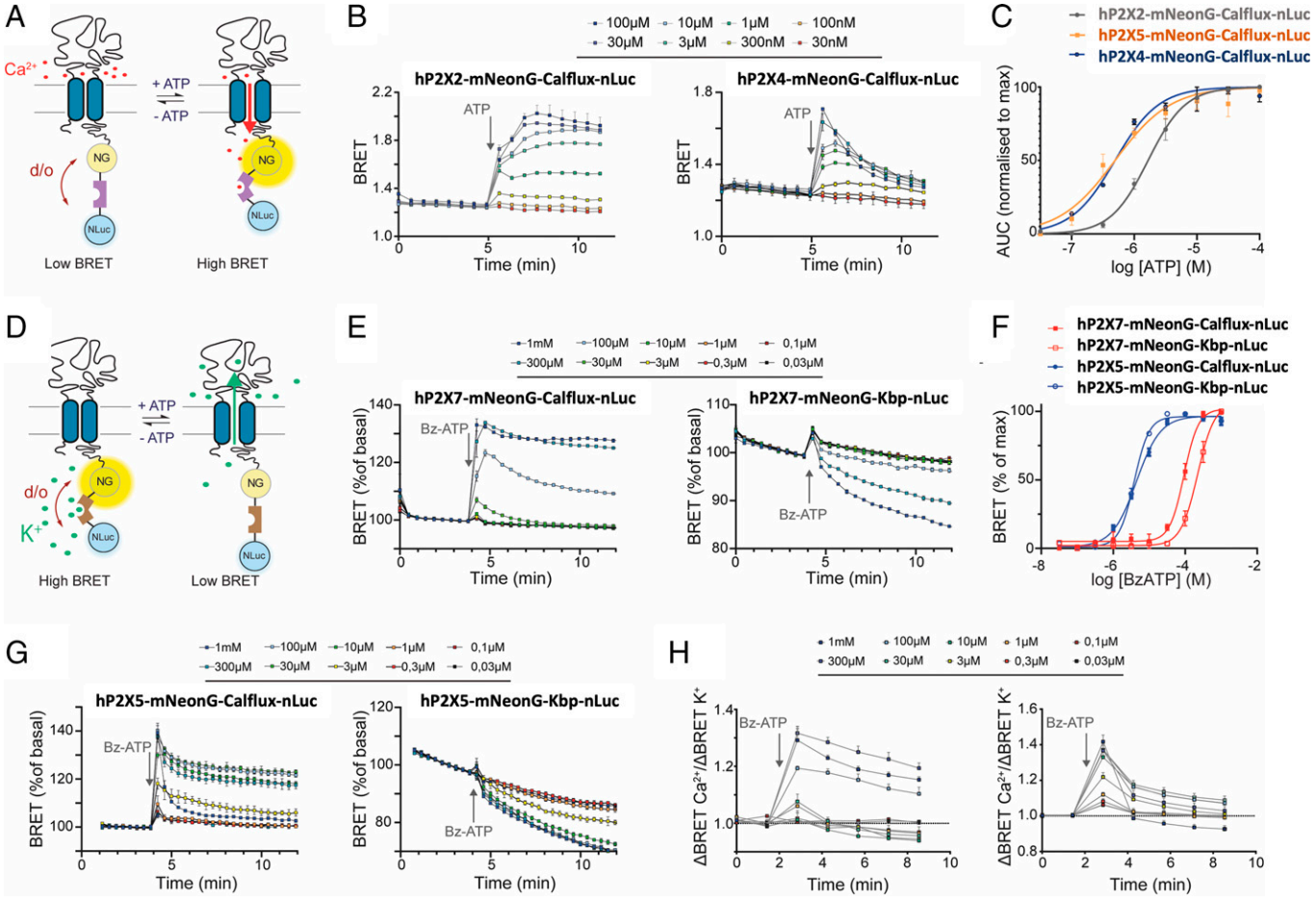

Fig. 7. (*A*) Schematic of the P2X-mNeonG-Calflux-nLuc BRET probe, where the mNeonG-Calflux-nLuc calcium biosensor was fused to the C-terminal extremity of P2X subunits. The opening of P2X receptor pores by ATP was expected to modify the distance (d) and/or orientation (o) between mNeonG and nLuc following calcium binding and conformational changes in Calflux. (*B*) Representative kinetics of the effect of increasing doses of ATP on the BRET ratio measured in HEK293T cells expressing the hP2X2-mNeonG-Calflux-nLuc (*Left*) or hP2X4-mNeonG-Calflux-nLuc (*Right*) BRET probes. (*C*) Concentration–response curves of ATP on the BRET ratio measured in HEK293T cells transfected with different human (h) P2X-mNeonG-Calflux-nLuc BRET probes ($n = 3$, except for hP2X4, $n = 2$). (*D*) Schematic of the P2X-mNeonG-Kbp-nLuc BRET probe, where the potassium biosensor mNeonG-Kbp-nLuc was fused to the C-terminal extremity of P2X subunits. The opening of P2X receptor pores by ATP was expected to modify the distance (d) and/or orientation (o) between mNeonG and nLuc following potassium efflux and conformational changes in Kbp. (*E* and *G*) Representative kinetics of the effect of increasing doses of Bz-ATP on the BRET ratio measured in HEK293T cells expressing the hP2X7 (*E*) or hP2X5 (*G*) subunits fused to either mNeonG-Calflux-nLuc (*Left*) or mNeonG-Kbp-nLuc (*Right*) BRET probes. (*F*) Concentration–response curves of Bz-ATP on the BRET ratio measured in HEK293T cells transfected with hP2X5 or hP2X7 and fused to either the calcium or the potassium BRET probes ($n \geq 3$). (*H*) Relative variation of the intracellular quantity of Ca^{2+} and K^+ in the vicinity of the P2X7 pore (*Left*) or P2X5 pore (*Right*).

determinants (43), these experiments nevertheless demonstrate that the sequence motif and charge distribution in the putative pore region determine the permeation properties of these TRP channels. It is also known that the TRPV1 pore is subjected to high plasticity during pore opening with proton and ligands, involving allosteric coupling between upper and lower gates and large conformational changes (45, 46). Given the similarity between the TRPV1 and KscA selectivity filters, and setting aside pore dilation, ligand-induced allosteric stabilization of distinct conformational states with subtle changes in charge distribution along the selectivity filter potentially may cause selective ion dehydration at the entrance barrier and/or more-or-less tortuous trajectories of different ions through the filter (47). It follows that TRPV1 ion channels should not be modeled as two-state biophysical entities, shuttling between open and closed states, but rather as allosteric, flexible entities, generating a variety of conformations in response to different ligands and activation modes. This model is closely related to the concept of "allosteric microprocessors" described by Smith et al. (48), where G protein–coupled receptor (GPCR)-biased ligands transmit distinct structural information that is processed into distinct biological outputs.

We moreover postulate that the TRPV1-dependent hyperpolarization measured when AMG517 was injected alone resulted from its activity as a partial agonist of the K^+ efflux. However, we acknowledge that our study was performed in HEK293T cells, with a resting membrane potential around −25 mV. At this value, the K^+ driving force is far from negligible since the electrochemical equilibrium potential of K^+ is around −90 mV. Knowing that most quiescent primary cells have a hyperpolarized resting membrane potential lower than −50 mV (such as neurons or pancreatic β-cells) (49), it may, therefore, be inferred that ligand bias on TRP ion channels will rarely have a physiological impact, as the K^+ driving force will not be strong enough in these cells. Nonetheless, since excitable cell depolarization during spontaneous spiking will induce a K^+-driving force, biased-enhanced K^+ permeability should reduce cellular input resistance and create a shunt that may powerfully hinder spontaneous spiking or bursting. Also, given the role that TRPV1 may play in the regulation of cancerous and healthy cell proliferation (50–52), and knowing that membrane depolarization is a prerequisite for cell division and proliferation (53), biased cationic selectivity in TRP ion channels may therefore occur in TRPV1 depending on the cell proliferation

state. Finally, it is well known that hyperthermia occurs in a variety of mammalian organisms, including human, mouse, and rat, following systemic administration of many of the TRPV1 antagonists, including BCTC and AMG517. In contrast, TRPV1 agonists (such as CAPS) and other antagonists (e.g., A-1165901, A-425619, AMG7905, and AMG8562) trigger hypothermia (reviewed in ref. 54). Whether ligand-biased cationic selectivity is a key factor in TRPV1-dependent body-temperature regulation remains to be determined.

Another intriguing issue arising from our results is that when extracellular Ca^{2+} is absent, K^+ apparently leaks freely from the nonactivated TRPV1 channel (Fig. 6). Reciprocally, in CAPS-activated HEK293T cells expressing rat TRPV1, Ahern et al. reported an E_{rev} shift to more positive values when the I/V curves were measured in the presence of a high concentration of Ca^{2+} (100 mM) (55). Altogether, these observations suggest that extracellular Ca^{2+} and intracellular K^+ compete to flow through the TRPV1 pore or that extracellular Ca^{2+} stabilizes a TRPV1 conformation less permeable to potassium.

In this study, we also generated biosensors to monitor the dynamic change of K^+ and Ca^{2+} ion concentration in the vicinity of the P2X ligand–gated ion-channel pore during activation. Although a comparison of selective calcium permeability between P2X receptors has been reported (56), selective permeability to various cations following activation of a given P2X receptor has never been demonstrated. Using our BRET biosensors, we found that, during the first few minutes after injection into the cell culture medium, Bz-ATP displayed similar potency to induce both K^+ efflux and Ca^{2+} influx through the hP2X5 receptor pore. However, Bz-ATP had higher potency to induce Ca^{2+} influx rather than K^+ efflux through the hP2X7 pore. This pointed to ligand bias-induced ion selectivity in hP2X7 channel. Interestingly, we also measured a time-dependent variation in hP2X5 and hP2X7 selectivity for potassium while Bz-ATP remained in the cell culture medium. Further research will focus on extending this concept to other P2X ion channels, such as the P2X4 receptor that displays the highest Ca^{2+} permeability among that family.

Finally, the demonstration that some compounds more potently inhibit or activate one specific ion flux may directly impact our TRP channel molecular pharmacology and drug screening approach. The gold standard for studying ion channel activity, including TRP and P2X, remains patch-clamp electrophysiology. While manual patch clamp is time consuming and requires expert handling, the advent of automated patch clamp (APC) increases throughput for screening ion channel targets (57). However, since APC remains expensive, the combination of fluorescence-based technologies, as a primary screen, followed by APC hit confirmation screen, has become the most commonly used method for ion channel–targeted drug discovery (58). In addition, TRP ion channel permeability to Ca^{2+} is remarkably high, which has favored the use of Ca^{2+}-based fluorescence assays to measure channel function using conventional plate readers or microscopes (59). Furthermore, whether APC is used as a primary or secondary screen, given the outward rectifying properties of many TRP channels, such as TRPV1/3/4, TRPA1, or TRPM8, most high-throughput screening studies only take into account their outward current measured at high positive membrane potential (60). While the amplitude of this current is much greater than the inward current measured at negative resting E_m, it nonetheless corresponds to an outward potassium current under nonphysiological membrane voltage conditions. We recently demonstrated the fallacy of the assumption that any hit displays an equal ability to activate or inhibit TRPV1 gating, irrespective of membrane potential (22). In this earlier study, we hypothesized that different ternary or quaternary conformational states of TRPV1 were stabilized when the E_m was clamped at selected values. The results presented here show that some compounds, such as AMG517, may behave as biased ligands, positively or negatively discriminating between ions flowing through a gated channel, thus adding a new layer of complexity. This highlights the risk of considering that all hits display an equal ability to activate or inhibit Ca^{2+} and K^+ fluxes (and probably the Na^+ flux as well). Ligand-dependent differential selectivity may, therefore, be a major source of experimental bias in many ion-channel drug screening campaigns. For example, if the workflow of a TRP ion-channel drug screening campaign includes APC confirmation of hits previously identified using a fluorescent calcium assay, there is a risk of false-negative hits if only the outward current is taken into account during the secondary screen. Similarly, it is perfectly conceivable that biased ligands may be overlooked during a primary screen for a specific nonselective cationic TRP ion channel if we consider only the calcium fluorescent assay results or APC results measured at only one membrane potential. Finally, there is also a risk of false-negative hits if ligand bias is not taken into account during a counterscreen to detect potential cross-reactivity of a third-party receptor/channel ligand on a cation channel such as TRP or P2X.

Therefore, in addition to our recently reported intra- and intermolecular BRET probes, these custom-engineered BRET-based probes now open up avenues for adding value to ion-channel drug discovery platforms by taking ligand bias into account, thus addressing molecular events related to ion channel activation (ligand bias, conformational changes, and protein–protein interaction dynamics) that are intractable using either conventional fluorescent-based probes or patch-clamp techniques (21, 22).

Materials and Methods

Plasmids. To generate the BRET constructs, mNeonGreen and nanoluciferase were used to improve the brightness of the assay and are referred to as mNeonG and nLuc for short in the rest of this paper. The mammalian expression vectors encoding mNeonG-TRPV1-nLuc, TRPV1-nLuc, and mNeonG-CaM were described in ref. 22.

Mammalian expression vectors for the expression of the nLuc-ion_sensor-mNeonG or mNeonG-ion_sensor-nLuc fusion proteins were constructed using cDNA bricks, obtained by gene synthesis (Genescript), that encode, respectively, nLuc or mNeonG (bricks 1.1, 1.3, 4.1, and 4.3), any ion sensor described in the text (Calflux, Kbp, or I3S, brick 1.2/4.2), and TRPV1 ion channel (bricks 2 and 3) as indicated in *SI Appendix*, Fig. 7. All bricks sequences are given in Dataset S1. hP2X DNA sequences were produced by gene synthesis and subcloned in pWPT EF1a. A *Pme*I site located at the C terminus of the P2X subunit was used to insert mNeonG-Calflux-nLuc or mNeonG-Kbp-nLuc in frame of the plasmids mentioned above.

Using the BsmB1 type IIS enzyme and T4 DNA ligase, the cDNA bricks were assembled in frame and in the right order into the pcDNA3.1(+)-Lac Z vector, which allowed direct visualization of the assembly efficiency using a colorimetric test based on alpha complementation (22). Briefly, a ligation mix containing 2 μL of T4 DNA ligase buffer 10×, 1 U of BsmBI enzyme, 1 U of T4 DNA ligase, 0.4 mM ATP, 4 mM dithiothreitol, 200 ng of the pcDNA3.1(+)-Lac Z vector, and 100 ng of bricks 1 through 4 was subjected to 35 cycles alternating two steps (step 1: 37 °C for 1 min, step 2: 16 °C for 1 min) before the enzymes were inactivated for 5 min at 55 °C. The ligation mix was then used to transform competent *Escherichia coli* DH5α by thermal shock.

Reagents. EGTA, olvanil, RTX, AMG517, AMG9810, BCTC, JNJ-17203212, and AMG21629 were all from Tocris. CAPS, CPZ, ATP, and Bz-ATP were from Sigma-Aldrich. Coelenterazine H (Nanolight Technology) was added to a final concentration of 5 μM.

Cell Culture and Transfections for BRET Assays. HEK293T cells were maintained in Dulbecco's modified Eagle's medium high glucose (Cat. No. D6429; Sigma-Aldrich) supplemented with 10% fetal bovine serum, 100 units mL^{-1} penicillin, and streptomycin.

All BRET assays were performed in 96-well plates. Twenty-four hours before transfection, cells were seeded at a density of 500,000 cells in 6-well dishes. Transient transfections were performed using polyethylenimine (PEI, linear, M_r 25,000; Cat. No. 23966 Polysciences) with a PEI/DNA ratio of 4:1, as explained in Percherancier et al. (61). When BRET assays were performed using any ion BRET sensor N-terminally or C-terminally fused to either TRPV1 or P2X 2/4/5/7 (*SI Appendix*, Fig. 2), HEK293T cells were transfected with 0.025 μg of the corresponding expression vector and 2 μg of the empty pcDNA3.1(+) vector. Alternatively, HEK293T cells were transfected with 0.1 μg of mNeonG-TRPV1-nLuc and 1.9 μg of empty pcDNA3.1(+) vector, or 0.1 μg of TRPV1-nLuc expression vector and 1.9 μg of mNeonG-CaM expression vectors for intramolecular and intermolecular BRET assays, respectively, as described in ref. 22. Following overnight incubation, transfected cells were detached and resuspended in Dulbecco's Modified Eagle Medium (DMEM) w/o Red-phenol (Cat. No. 21063-029; Thermo Fisher Scientific) containing 10% fetal bovine serum and 100 units mL^{-1} penicillin and streptomycin before being seeded at 10^5 cells per well in 96-well white plates (Cat. No. 655083, Greiner Bio-One). Cells were left in culture for an additional 24 h before being processed for BRET assay.

BRET Measurement in 96-Well Plates. All BRET measurements were performed in Red-phenol-free cell culture medium, except for experiments described in Fig. 4, performed using an isotonic solution ("buffer with Ca^{2+}": 145 mM NaCl, 5 mM KCl, 4 mM KH_2PO_4, 1 mM $CaCl_2$, 1 mM $MgSO_4$, 10 mM glucose, pH 7.4). When indicated, $CaCl_2$ was either replaced by 2 mM EGTA ("buffer with EGTA") or by 1 mM $BaCl_2$ ("buffer with Ba^{2+}"), or NaCl was replaced by 145 mM NMDG. Following the addition of 5 μM coelenterazine H into the extracellular medium, bioluminescent signals were measured using a multidetector TriStar2 LB942 microplate reader (Berthold Technologies) and emission filters centered at 515 ± 20 nm for mNeonG and 460 ± 20 nm for nLuc.

The BRET signal was determined by calculating the ratio of the emission intensity measured in the acceptor window (I_{mNeonG}) over the emission intensity measured in the donor window (I_{nLuc}), according to Eq. **1**:

$$\text{BRET} = \frac{\text{I}_{\text{mNeonG}}}{\text{I}_{\text{nLuc}}}. \quad [1]$$

Due to the overlapping emission spectra of nLuc and mNeonG, a fraction of the light detected in the mNeonG filter originates from the nLuc emission, resulting in a contaminating signal (62). In that configuration, the net BRET was therefore defined as the BRET ratio of cells coexpressing nLuc and mNeonG constructs minus the BRET ratio of cells expressing only the nLuc construct in the same experiment.

To assess the functionality of any ion channel BRET-based probes, coelenterazine H was added at the concentration of 5 μM and incubated 10 min before agonists and antagonists were injected. BRET signals were measured 5 min after the addition of the last compound. All experiments were performed at 37 °C and pH 7.4 unless otherwise indicated. In all experiments, dimethylsulfoxide (DMSO) alone was used negative control (vehicle).

BRET data processing and statistical analysis. Concentration–response curves, kinetics, and statistics were analyzed using the software Prism 8.01 (GraphPad Software). Sigmoidal dose–response curves were fitted using Eq. **2**:

$$\text{Y} = \text{Bottom} + \frac{(Top - Bottom)}{1 + 10^{logEC50 - X}}, \quad [2]$$

where X is the logarithm of agonist concentration and Y is the response; bottom is the Y value at the bottom plateau; top is the Y value at the top plateau; and Log EC_{50} is the X value when the response is halfway between bottom and top.

A *t* test corrected for multiple comparisons using the Holm-Šídák method was used to assess the statistical significance of the difference calculated between two set of EC_{50}/IC_{50} values.

Membrane Potential Assay Kits in Confocal Microscopy. Transfected HEK293T cells plated in 96 well black plates with clear bottom (Cat. No. 655090, Greiner Bio-One) were used for real-time fluorescence imaging of the membrane potential. To prepare the membrane potential assay, the FLIPR Red Assay explorer-kit reagents were prepared according to the manufacturer's instructions (Molecular Device). On the day of the experiment, the culture medium was replaced with 50 μL of fresh DMEM (Sigma-Aldrich). Then, 50 μL of red dye-loading buffer was added directly to each well and left for 30 min at 37 °C. Image acquisition was acquired using a Nikon D-Eclipse C1 confocal scanning microscope (image acquisition frequency 0.25 Hz, excitation wavelengths: 561 nm emission wavelengths: 605 nm). For each independent experiment, 20 fields were acquired.

Manual Patch Clamp. For whole-cell electrophysiological experiments assessing that the CAPS-induced whole-cell current was of similar magnitude in HEK293T cells expressing either YFP-TRPV1 or mNeonG-Calflux-nLuc-TRPV1 (Fig. 2*B*), the transiently transfected HEK293T cells were bathed in an extracellular medium containing 135 mM NaCl, 5 mM CsCl, 1 mM $MgCl_2$, 1 mM $CaCl_2$, 10 mM glucose, and 10 mM Hepes, pH 7.4 adjusted with NaOH. The recording patch-clamp pipette was filled with artificial intracellular saline containing: 130 mM CsCl, 5 mM EGTA, 5.5 mM $MgCl_2$, 5 mM Na_2ATP, and 5 mM Hepes (290 mOsm adjusted with mannitol and pH 7.2 adjusted with KOH).

For all other whole-cell electrophysiological experiments (*SI Appendix*, Figs. 4 and 6), the following extracellular media were used as indicated in the text:

- Buffer with Ca^{2+}: 130 mM NaCl, 5.6 mM KCl, 2 mM $CaCl_2$, 1 mM $MgCl_2$, 8 mM Hepes, 11 mM glucose and pH 7.4 adjusted with NaOH.
- Buffer with EGTA: 130 mM NaCl, 5.6 mM KCl, 0.5 mM EGTA, 1 mM $MgCl_2$, 8 mM Hepes, 11 mM glucose and pH 7.4 adjusted with NaOH.
- Buffer with NMDG: 130 mM NMDG, 5.6 mM KCl, 2 mM $CaCl_2$, 1 mM $MgCl_2$, 8 mM Hepes, 11 mM glucose and pH 7.4 adjusted with NaOH.
- Buffer with NMDG and EGTA: 130 mM NMDG, 5.6 mM KCl, 0.5 mM EGTA, 1 mM $MgCl_2$, 8 mM Hepes, 11 mM glucose and pH 7.4 adjusted with NaOH.

In all these experiments, the intracellular medium was composed of 145 mM KCl, 2 mM $MgCl_2$, and 10 mM Hepes (pH 7.3 adjusted with KOH).

For all experiments, the osmolarity (measured with a cryo-osmometer type 15 Löser) of the external salt solution was adjusted to 300 mOsm with mannitol and pH adjusted as indicated.

Cells were viewed under phase contrast using a Nikon Diaphot inverted microscope. Borosilicate glass micropipettes (GC150F-10, Harvard Apparatus, Phymep) were pulled with a DMZ-Universal puller. The pipettes had a mean resistance of 4 MΩ when measured under standard recording conditions. An RK-400 patch-clamp amplifier (Biologic) was used for whole-cell recordings. Stimulus control, data acquisition, and processing were carried out on a PC fitted with a Digidata 1200 interface, using the pCLAMP 10.7 software (Molecular Devices). Current records were filtered using a Bessel filter at 1 kHz and digitized for storage and analysis. Recordings were performed in voltage-clamp and whole-cell configurations to measure global currents. After the seal, a resting potential of −65 mV was imposed, and 650-ms voltage ramps were applied every 10 s for 3 min. When indicated, after four ramps, capsaicin (10 μM) or EGTA (500 μM) was applied to the recorded cell by pressure ejection from a glass pipette located close to the cell. CAPS/EGTA-activated currents were determined by the difference between maximal induced current and average current before ejection.

Automated Patch-Clamp Assay. Automated patch-clamp assays were outsourced to SB Drug Discovery. Briefly, automated patch-clamp recordings were performed using the SyncroPatch 384PE (Nanion) and HEK293T cell line stably expressing human TRPV1 (SB Drug Discovery) that were plated 24 h before the experiment and incubated at 37 °C and 5% CO_2. The voltage protocol generation and data collection were performed with the PatchController384 V1.6.6 and Data Controller V1.6.0.

The protocol consisted of two applications of external solution (control period) containing 140 mM NaCl, 4 mM KCl, 2 mM CaCl2, 1 mM MgCl2, 10 mM Hepes, and 5 mM glucose, at pH 7.4, followed by the addition of one application of the agonist capsaicin EC_{50} (100 nM) for 1 to 2 min, followed by the addition of 10 μM of the test compound (1 to 2 min), in the presence of capsaicin EC_{50}, and lastly the addition of the full block 10 μM capsazepine (1 min). The current was monitored using a ramp protocol from −100 mV to +100 mV over 300 ms, from a holding potential of −60 mV, which was repeated every 20 s. In each condition, the maximum DMSO concentration at the end of the run was 0.3%.

Data, Materials, and Software Availability. All study data are included in the article and/or supporting information.

ACKNOWLEDGMENTS. The research leading to these results received funding from 1) Aquitaine Science Transfert, the Technology Transfer Accelerator Office of New Aquitaine (France), 2) the French National Research Agency (ANR) under grant agreement ANR-19-CE44-0010-02 (the CANALBRET project), and 3) the New Aquitaine regional council under grant agreement AAPR2020I-2019-8140410 (The PHYSTRIG project). We thank Bernard Veyret for his wise advice and proof-reading of the manuscript.

Author affiliations: [a]Laboratory of Integration from Materials to System, CNRS UMR 5218, University of Bordeaux, Talence, F-33400 France; [b]Institute of Functional Genomics, CNRS, INSERM UMR 5203, University of Montpellier, Montpellier, F-34094 France; and [c]Centre de Recherche Cardio-Thoracique de Bordeaux, INSERM U1045, University of Bordeaux, Pessac, F-33600 France

Author contributions: Y.L.C., T.D., J.-F.Q., V.C., and Y.P. designed research; Y.L.C., S.P., A.J., P.M., A.G., A.C., S.B., F.P.D.G., A.H., I.L., T.D., J.-F.Q., V.C., and Y.P. performed research; Y.L.C., S.P., A.J., P.M., A.G., T.D., J.-F.Q., V.C., and Y.P. contributed new reagents/analytic tools; Y.L.C., S.P., A.J., P.M., A.G., T.D., J.-F.Q., V.C., and Y.P. analyzed data; and Y.L.C., A.G., T.D., J.-F.Q., V.C., and Y.P. wrote the paper.

1. L. Kiss, J. LoTurco, S. J. Korn, Contribution of the selectivity filter to inactivation in potassium channels. *Biophys. J.* **76**, 253–263 (1999).
2. J. G. Starkus, L. Kuschel, M. D. Rayner, S. H. Heinemann, Ion conduction through C-type inactivated Shaker channels. *J. Gen. Physiol.* **110**, 539–550 (1997).
3. F. C. Chatelain *et al.*, TWIK1, a unique background channel with variable ion selectivity. *Proc. Natl. Acad. Sci. U.S.A.* **109**, 5499–5504 (2012).
4. L. Ma, X. Zhang, H. Chen, TWIK-1 two-pore domain potassium channels change ion selectivity and conduct inward leak sodium currents in hypokalemia. *Sci. Signal.* **4**, ra37 (2011).
5. L. Ma, X. Zhang, M. Zhou, H. Chen, Acid-sensitive TWIK and TASK two-pore domain potassium channels change ion selectivity and become permeable to sodium in extracellular acidification. *J. Biol. Chem.* **287**, 37145–37153 (2012).
6. H. Chen, F. C. Chatelain, F. Lesage, Altered and dynamic ion selectivity of K+ channels in cell development and excitability. *Trends Pharmacol. Sci.* **35**, 461–469 (2014).
7. M.-K. Chung, A. D. Güler, M. J. Caterina, TRPV1 shows dynamic ionic selectivity during agonist stimulation. *Nat. Neurosci.* **11**, 555–564 (2008).
8. C. H. Munns, M.-K. Chung, Y. E. Sanchez, L. M. Amzel, M. J. Caterina, Role of the outer pore domain in transient receptor potential vanilloid 1 dynamic permeability to large cations. *J. Biol. Chem.* **290**, 5707–5724 (2015).
9. L. Peverini, J. Beudez, K. Dunning, T. Chataigneau, T. Grutter, New insights into permeation of large cations through ATP-gated P2X receptors. *Front. Mol. Neurosci.* **11**, 265 (2018).
10. L. G. B. Ferreira, R. X. Faria, TRPing on the pore phenomenon: What do we know about transient receptor potential ion channel-related pore dilation up to now? *J. Bioenerg. Biomembr.* **48**, 1–12 (2016).
11. A. E. López-Romero *et al.*, TRP ion channels: Proteins with conformational flexibility. *Channels (Austin)* **13**, 207–226 (2019).
12. M. Li, G. E. S. Toombes, S. D. Silberberg, K. J. Swartz, Physical basis of apparent pore dilation of ATP-activated P2X receptor channels. *Nat. Neurosci.* **18**, 1577–1583 (2015).
13. D. S. K. Samways, E. Tomkiewicz, O. M. Langevin, M. Bukhari, Measurement of relative Ca^{2+} permeability during sustained activation of TRPV1 receptors. *Pflugers Arch.* **468**, 201–211 (2016).
14. A. Garami *et al.*, Contributions of different modes of TRPV1 activation to TRPV1 antagonist-induced hyperthermia. *J. Neurosci.* **30**, 1435–1440 (2010).
15. J. Yang *et al.*, Coupling optogenetic stimulation with NanoLuc-based luminescence (BRET) Ca^{++} sensing. *Nat. Commun.* **7**, 13268 (2016).
16. H. Bischof *et al.*, Novel genetically encoded fluorescent probes enable real-time detection of potassium in vitro and in vivo. *Nat. Commun.* **8**, 1422 (2017).
17. B. Liu, B. Poolman, A. J. Boersma, Ionic strength sensing in living cells. *ACS Chem. Biol.* **12**, 2510–2514 (2017).
18. N. R. Gavva *et al.*, Repeated administration of vanilloid receptor TRPV1 antagonists attenuates hyperthermia elicited by TRPV1 blockade. *J. Pharmacol. Exp. Ther.* **323**, 128–137 (2007).
19. N. R. Gavva *et al.*, Pharmacological blockade of the vanilloid receptor TRPV1 elicits marked hyperthermia in humans. *Pain* **136**, 202–210 (2008).
20. S. Bevan *et al.*, Capsazepine: A competitive antagonist of the sensory neurone excitant capsaicin. *Br. J. Pharmacol.* **107**, 544–552 (1992).
21. H. J. Ruigrok *et al.*, Full-spectral multiplexing of bioluminescence resonance energy transfer in three TRPV channels. *Biophys. J.* **112**, 87–98 (2017).
22. Y. Chappe *et al.*, High-throughput screening of TRPV1 ligands in the light of the bioluminescence resonance energy transfer technique. *Mol. Pharmacol.* **100**, 237–257 (2021).
23. M. J. Caterina *et al.*, The capsaicin receptor: A heat-activated ion channel in the pain pathway. *Nature* **389**, 816–824 (1997).
24. Y. Cui *et al.*, Selective disruption of high sensitivity heat activation but not capsaicin activation of TRPV1 channels by pore turret mutations. *J. Gen. Physiol.* **139**, 273–283 (2012).
25. V. De-la-Rosa, G. E. Rangel-Yescas, E. Ladrón-de-Guevara, T. Rosenbaum, L. D. Islas, Coarse architecture of the transient receptor potential vanilloid 1 (TRPV1) ion channel determined by fluorescence resonance energy transfer. *J. Biol. Chem.* **288**, 29506–29517 (2013).
26. B. Liu *et al.*, Design and properties of genetically encoded probes for sensing macromolecular crowding. *Biophys. J.* **112**, 1929–1939 (2017).
27. M. Tominaga, M. Wada, M. Masu, Potentiation of capsaicin receptor activity by metabotropic ATP receptors as a possible mechanism for ATP-evoked pain and hyperalgesia. *Proc. Natl. Acad. Sci. U.S.A.* **98**, 6951–6956 (2001).
28. W. Fischer, H. Franke, H. Gröger-Arndt, P. Illes, Evidence for the existence of P2Y1,2,4 receptor subtypes in HEK-293 cells: Reactivation of P2Y1 receptors after repetitive agonist application. *Naunyn Schmiedebergs Arch. Pharmacol.* **371**, 466–472 (2005).
29. E. Cao, Structural mechanisms of transient receptor potential ion channels. *J. Gen. Physiol.* **152**, e201811998 (2020).
30. L. Vyklický, *et al.*, Calcium-dependent desensitization of vanilloid receptor TRPV1: A mechanism possibly involved in analgesia induced by topical application of capsaicin. *Physiol. Res.* **57**, 10 (2008).
31. A. Jara-Oseguera, C. Bae, K. J. Swartz, An external sodium ion binding site controls allosteric gating in TRPV1 channels. *eLife* **5**, e13356 (2016).
32. T. Ohta, T. Imagawa, S. Ito, Novel gating and sensitizing mechanism of capsaicin receptor (TRPV1): Tonic inhibitory regulation of extracellular sodium through the external protonation sites on TRPV1. *J. Biol. Chem.* **283**, 9377–9387 (2008).
33. J. Winter, A. Dray, J. N. Wood, J. C. Yeats, S. Bevan, Cellular mechanism of action of resiniferatoxin: A potent sensory neuron excitotoxin. *Brain Res.* **520**, 131–140 (1990).
34. V. Ralevic, D. A. Kendall, J. C. Jerman, D. N. Middlemiss, D. Smart, Cannabinoid activation of recombinant and endogenous vanilloid receptors. *Eur. J. Pharmacol.* **424**, 211–219 (2001).
35. B. R. Bianchi *et al.*, Modulation of human TRPV1 receptor activity by extracellular protons and host cell expression system. *Eur. J. Pharmacol.* **537**, 20–30 (2006).
36. N. R. Gavva *et al.*, The vanilloid receptor TRPV1 is tonically activated in vivo and involved in body temperature regulation. *J. Neurosci.* **27**, 3366–3374 (2007).
37. N. R. Gavva *et al.*, Gavva 2005 J Pharmacol Exp Ther -AMG 9810 [(iE-i) -3-(4- it-i -Butylphenyl)- iN-i -(2,3-dihydrobenzo [ib-i] [1,4].pdf. *J. Pharmacol. Exp. Ther.* **313**, 474–484 (2005).
38. A. A. Ramahi and R. L. Ruff, in Encyclopedia of the Neurological Sciences, ed. M. J. Aminoff and R. B. Daroff, Academic Press, Oxford, 2nd edn, 2014, pp. 1034–1035.
39. R. D. Kirkton, N. Bursac, Engineering biosynthetic excitable tissues from unexcitable cells for electrophysiological and cell therapy studies. *Nat. Commun.* **2**, 300 (2011).
40. S. J. Fountain, R. A. North, A C-terminal lysine that controls human P2X4 receptor desensitization. *J. Biol. Chem.* **281**, 15044–15049 (2006).
41. L. E. Browne, V. Compan, L. Bragg, R. A. North, P2X7 receptor channels allow direct permeation of nanometer-sized dyes. *J. Neurosci.* **33**, 3557–3566 (2013).
42. G. Owsianik, K. Talavera, T. Voets, B. Nilius, Permeation and selectivity of TRP channels. *Annu. Rev. Physiol.* **68**, 685–717 (2006).
43. C. García-Martínez, C. Morenilla-Palao, R. Planells-Cases, J. M. Merino, A. Ferrer-Montiel, Identification of an aspartic residue in the P-loop of the vanilloid receptor that modulates pore properties. *J. Biol. Chem.* **275**, 32552–32558 (2000).
44. T. Voets *et al.*, Molecular determinants of permeation through the cation channel TRPV4. *J. Biol. Chem.* **277**, 33704–33710 (2002).
45. K. Zhang, D. Julius, Y. Cheng, Structural snapshots of TRPV1 reveal mechanism of polymodal functionality. *Cell* **184**, 5138–5150.e12 (2021).
46. E. Cao, M. Liao, Y. Cheng, D. Julius, TRPV1 structures in distinct conformations reveal activation mechanisms. *Nature* **504**, 113–118 (2013).
47. K. Mita *et al.*, Conductance selectivity of Na^+ across the K^+ channel via Na^+ trapped in a tortuous trajectory. *Proc. Natl. Acad. Sci. U.S.A.* **118**, e2017168118 (2021).
48. J. S. Smith, R. J. Lefkowitz, S. Rajagopal, Biased signalling: From simple switches to allosteric microprocessors. *Nat. Rev. Drug Discov.* **17**, 243–260 (2018).
49. L. Abdul Kadir, M. Stacey, R. Barrett-Jolley, Emerging roles of the membrane potential: Action beyond the action potential. *Front. Physiol.* **9**, 1661 (2018).
50. J. K. Bujak, D. Kosmala, I. M. Szopa, K. Majchrzak, P. Bednarczyk, Inflammation, cancer and immunity-implication of TRPV1 channel. *Front. Oncol.* **9**, 1087 (2019).
51. K. Zhai, A. Liskova, P. Kubatka, D. Büsselberg, Calcium entry through TRPV1: A potential target for the regulation of proliferation and apoptosis in cancerous and healthy cells. *Int. J. Mol. Sci.* **21**, 4177 (2020).
52. K. S. Vrenken, K. Jalink, F. N. van Leeuwen, J. Middelbeek, Beyond ion-conduction: Channel-dependent and -independent roles of TRP channels during development and tissue homeostasis. *Biochim. Biophys. Acta* **1863** (6 Pt B), 1436–1446 (2016).
53. J. Carvalho, A bioelectric model of carcinogenesis, including propagation of cell membrane depolarization and reversal therapies. *Sci. Rep.* **11**, 13607 (2021).
54. A. Garami *et al.*, Hyperthermia induced by transient receptor potential vanilloid-1 (TRPV1) antagonists in human clinical trials: Insights from mathematical modeling and meta-analysis. *Pharmacol. Ther.* **208**, 107474 (2020).
55. G. P. Ahern, I. M. Brooks, R. L. Miyares, X. B. Wang, Extracellular cations sensitize and gate capsaicin receptor TRPV1 modulating pain signaling. *J. Neurosci.* **25**, 5109–5116 (2005).
56. T. M. Egan, B. S. Khakh, Contribution of calcium ions to P2X channel responses. *J. Neurosci.* **24**, 3413–3420 (2004).
57. A. Obergrussberger, S. Friis, A. Brüggemann, N. Fertig, Automated patch clamp in drug discovery: Major breakthroughs and innovation in the last decade. *Expert Opin. Drug Discov.* **16**, 1–5 (2021).
58. H. B. Yu, M. Li, W. P. Wang, X. L. Wang, High throughput screening technologies for ion channels. *Acta Pharmacol. Sin.* **37**, 34–43 (2016).
59. C. Cordero-Sánchez, I. Mudarra-Fraguas, A. Fernández-Carvajal, "Fluorescence-based functional assays for Ca2+-permeable thermoTRP channels" in *TRP Channels, Methods in Molecular Biology*, A. Ferrer-Montiel, T. Hucho, Eds. (Springer New York, 2019), pp. 99–110.
60. J.-M. M. Chambard, E. Tagat, P. Boudeau, M. Partiseti, Transforming TRP channel drug discovery using medium-throughput electrophysiological assays. *J. Biomol. Screen.* **19**, 468–477 (2014).
61. Y. Percherancier *et al.*, Bioluminescence resonance energy transfer reveals ligand-induced conformational changes in CXCR4 homo- and heterodimers. *J. Biol. Chem.* **280**, 9895–9903 (2005).
62. F. F. Hamdan, Y. Percherancier, B. Breton, M. Bouvier, Monitoring protein-protein interactions in living cells by bioluminescence resonance energy transfer (BRET). *Curr. Protoc. Neurosci.* **Chapter 5**, Unit 5.23 (2006).